



8th International Congress of Information and Communication Technology, ICICT 2019

A Study on Dynamic Measurement System of Contact Wire Wear in Electrified Railway

Cheng Xi You^{*a*}

China Railway Guangzhou Administration Group Co.,Ltd., No.151 Zhongshanyi Road, Guangzhou 510088, China

Abstract

As the tension of contact wire in high-speed electrified railway increases greatly, coupled with the fast relative speed of pantograph and catenary, the wear of contact wire is more serious. Timely and accurate measurement of contact wire wear becomes increasingly important. In this paper a dynamic measurement method for contact wire wear in electrified railway is introduced. With the aid of laser supplementary light, the bottom of contact wire is captured by line-scanning camera. The measurement is performed based on the principle of binocular ranging by analyzing the local wear conditions captured with different cameras to calculate the complete wear data of contact wire. The method has been tested on line, and the test data shows that the goal of quickly measuring the contact wire wear is achieved.

© 2019 The Authors. Published by Elsevier Ltd.

This is an open access article under the CC BY-NC-ND license (<https://creativecommons.org/licenses/by-nc-nd/4.0/>)

Selection and peer-review under responsibility of the 8th International Congress of Information and Communication Technology, ICICT 2019.

Keywords: contact wire; wear; dynamic measurement

1. Introduction

By the end of 2018, China's high-speed railway has exceeded 25,000 kilometers. With the development of high-speed electrified railway, the maintenance burden of power supply system has accordingly increased¹. During the construction of high-speed railway, in order to ensure the smoothness of OCS lines, the tension increases greatly and the elasticity decreases in the pantograph-catenary operation. Meanwhile, the relatively fast speed of pantograph-

* * Corresponding author. Tel.:+(86)18666095688

Email: youx2005@126.com

catenary in high-speed railway will inevitably lead to the increase of pantograph-catenary force and arc, and the severe wear of local contact wires². If without timely detection, it will result in wire breakage at serious wear positions on account of high tension force. At present, in China the wear is mainly measured by manual with vernier caliper and the workload of line inspection is so heavy³. Since the wear points are usually in discrete distribution and easy for missed measurement, if the wear of contact wire can be quickly and efficiently measured using on-board measurement equipment, it will be of great significance to prevent the pantograph and catenary accident and save the maintenance time of operation site.

Based on this reason, the principle of dynamic measurement of contact wire wear in high-speed railway and the developed measurement device are described in detail in this paper, and the data collected from the device are processed and analyzed to further confirm the practicability of the measurement technology.

2. Introduction to Measurement Principle

2.1. Measurement principle of the system

The system builds a three-dimensional model by finding the matching points on the two cameras. With these matching points and the distance between two cameras, the three-dimensional coordinate of the points in the image can be calculated.

The basic principle of system imaging⁴ is as below:

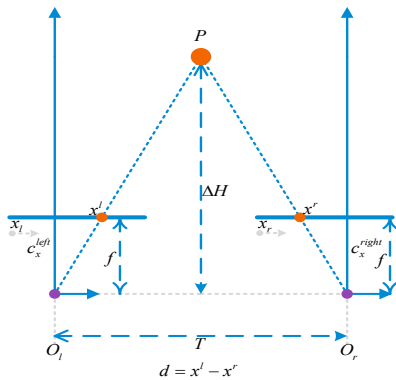


Fig. 1. Plane sketch of the system measurement principle

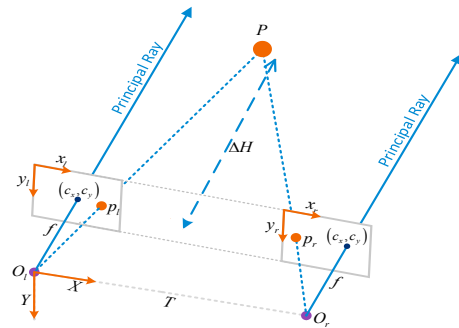


Fig. 2. Stereoscopic sketch of the system measurement principle

As shown in Fig. 1 and Fig. 2, the foci of the two cameras are O_l and O_r respectively. The parameters of the two cameras are exactly the same. The images taken are aligned row by row and the pixels are aligned completely. The imaging points of contact wire P on the images of the two cameras are P_l and P_r , f is the focal length of the camera, and T is the focal distance of the two cameras. From the triangle similarity principle, it can be concluded that:

$$\frac{T - (x_l - x_r)}{\Delta H - f} = \frac{\Delta H}{Z} \tag{1}$$

Where x_l and x_r are the corresponding X coordinates in the coordinate system created with the upper left corner of each image as the coordinate origin, and ΔH can be obtained from the following equation:

$$\Delta H = \frac{fT}{x_l - x_r} \tag{2}$$

Prior to the operation of the measuring system, it is required to calibrate the cameras by measuring the relative positions between the two cameras (that is, the rotation matrix R of the right camera relative to the left camera and

the translation vector t)⁵. Then the binocular correction is performed so that any point on one image has the same row number as its corresponding point on another image, and the corresponding point can be matched by one-dimensional search on that row⁶. In addition, the disparity map is obtained by matching the corresponding image points of the same scene in the left and right views, and the depth can be calculated through the above formula⁷.

2.2. Angle processing of contact wire wear

The linear array camera is mounted on the roof of the vehicle. The connecting line of mounting position is parallel to the pantograph contact strip, ensuring that no matter from what angle the pantograph contact strip contacts with the contact wire, the connecting line of the linear array camera can keep parallel to the wear section of contact wire as shown in Fig. 3.

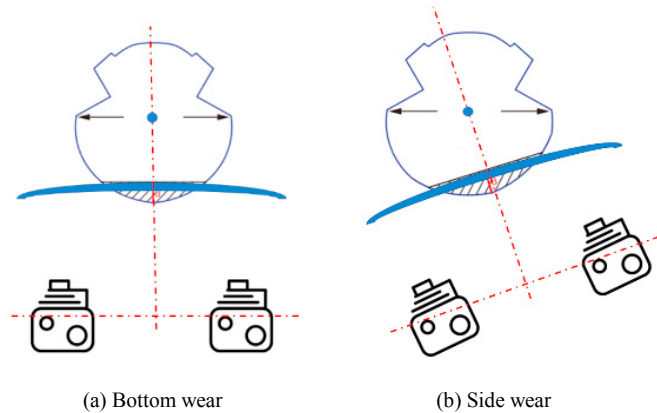


Fig. 3. Relative position relation between connecting line of linear array camera and wear surface of contact wire

3. System implementation

3.1. System hardware implementation

The contact wire wear measurement system is composed of contact wire wear acquisition system, data processing system and mileage positioning system as its structural diagram shown below:

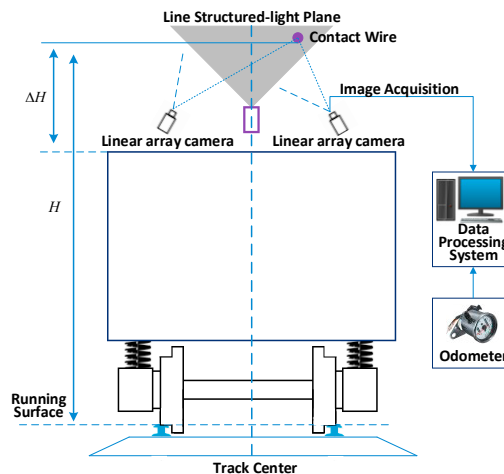


Fig.4. Structural diagram of contact wire wear measurement system

In the figure, H is the height of contact wire and ΔH is the height of contact wire relative to the top of measuring vehicle. The contact wire wear acquisition system consists of a set of linear array cameras and a line laser. The line structured lights are emitted from the line laser to intersect with the contact wire, which forms the laser stripe containing the contact wire profile information. In order to acquire the stripe image and transmit it to the data processing system for processing, it is required that two high-speed cameras are placed parallel to each other. Then the height of contact wire can be obtained with the parallax and internal and external parameters of two cameras based on the principle of triangular distance measurement.

Since the curvature of the contact wire wear surface is smaller than that of the non-wear area, according to the reflection law, the brightness of the wear surface in the image is more obvious than that of the non-wear area as shown in Fig.5. Therefore, the wear width can be extracted from the image via image processing technology, and the actual wear surface width can be calculated with the camera internal and external parameters and contact wire height. Finally, the corresponding wear depth can be calculated according to the inherent shape characteristics of the contact wire.

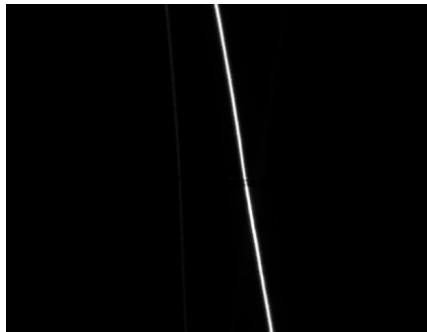


Fig.5. Imaging of contact wire

When measuring the contact wire wear dynamically, the photoelectric odometer mounted on the axle rotates with the wheel and sends the photoelectric pulse signal to the data processing system. Two cameras are triggered in turn by the measurement system to complete the image acquisition of OCS laser stripe at the same time. In addition, the mileage of measuring vehicle can be further calculated through the number of wheel revolutions recorded by the odometer so that the contact wire can be positioned.

3.2. Calibration and calculation

3.2.1 Calibration of binocular linear array camera

Using the binocular linear array camera for contact wire height measurement requires the calibration of internal and external parameters of two cameras. In this scheme, the structured light plane is coplanar with the vision plane of two cameras, so the axis is not calibrated. The imaging of binocular linear array camera imaging is shown in Fig.6.

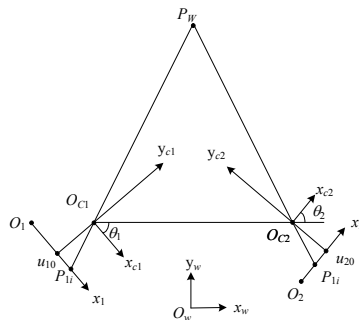


Fig.6. Imaging diagram of binocular linear array camera

In the figure, $O_w x_w y_w$ is the world coordinate system, $O_1 x_1$ and $O_2 x_2$ are the left and right camera image coordinate systems, $O_{c1} x_{c1} y_{c1}$ and $O_{c2} x_{c2} y_{c2}$ are the left and right camera coordinate systems. According to the imaging principle of linear array camera, a perspective transformation model of linear array camera can be established based on the camera pixel scale factor ∂_k and the principal point coordinate u_{k0} as shown in the equation (3):

$$y_{ck} \begin{bmatrix} x_k \\ 1 \end{bmatrix} = \begin{bmatrix} \partial_k & u_{k0} \\ 0 & 1 \end{bmatrix} \begin{bmatrix} x_{ck} \\ y_{ck} \end{bmatrix} \quad (3)$$

The transformation relation between world coordinate system and camera coordinate system is as below:

$$\begin{bmatrix} x_{ck} \\ y_{ck} \end{bmatrix} = R_k \begin{bmatrix} x_w \\ y_w \end{bmatrix} + t_k = \begin{bmatrix} \cos \theta_k & \sin \theta_k \\ -\sin \theta_k & \cos \theta_k \end{bmatrix} \begin{bmatrix} x_w \\ y_w \end{bmatrix} + \begin{bmatrix} t_{k1} \\ t_{k2} \end{bmatrix} \quad (4)$$

The mapping relation between image coordinate system and world coordinate system can be obtained via simultaneous equation (3) and (4).

$$y_{ck} \begin{bmatrix} x_k \\ 1 \end{bmatrix} = \begin{bmatrix} \partial_k \cos \theta_k - u_{k0} \sin \theta_k & \partial_k \sin \theta_k + u_{k0} \cos \theta_k \\ -\sin \theta_k & \cos \theta_k \end{bmatrix} \begin{bmatrix} x_w \\ y_w \end{bmatrix} + \begin{bmatrix} \partial_k t_{k1} + u_{k0} t_{k2} \\ t_{k2} \end{bmatrix} \quad (5)$$

In this paper, multiple sets of calibration data are collected, and multiple iterations are performed using the L-M algorithm to obtain the optimal solution of the internal and external parameters of the camera.

When measuring the contact wire height, the corresponding world coordinates can be calculated inversely by substituting the above parameters and the image pixel coordinates of left and right camera into the equation (5). Since the world coordinates are based on the roof surface, the height of contact wire is relative to the top of measuring vehicle.

3.2.2 Measurement and calculation of contact wire wear

In the same railway line, the model of contact wire is fixed, and in the same camera, the height of contact wire is inversely proportional to the width of contact wire in the image as shown in Fig.7. Therefore, the corresponding image width can be calculated according to the height of contact wire, and the wear surface width of contact wire can be further calculated. The actual wear surface width of contact wire is indicated in equation (6):

$$w = \frac{w' \Delta H dX}{f} \quad (6)$$

In the equation, w' is the wear surface width of contact wire, ΔH is the height of contact wire relative to the roof of vehicle, dX is the physical size of linear array camera pixel, and f is the focal distance of camera.

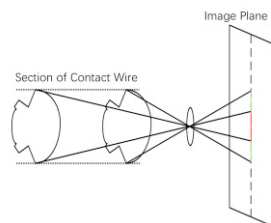


Fig.7. Schematic diagram of the relation between contact wire height and image size

The specific steps of measuring the wear surface width of contact wire are as below:

Step 1: Extract the edge from the contact wire image after distortion correction using the canny operator.

Step 2: Process the edge image morphologically to eliminate the voids between edges.

Step 3: Mark the connected domain to obtain the location of the suspected contact wire. Screening is required due to interference in objects such as tree branches, non-operating contact wire and catenary. The screening bases are as follows:

Brightness of connected domain. The contact wire wear surface is close to specular reflection and is brighter than the tree branch and non-wear contact wire in the image.

Tilt angle of connected domain. The contact wire is usually incident vertically, while the interferences such as branches are mostly projected horizontally.

Determination of interruption (discontinuity) of connected domain. In the image the contact wire is continuous, so the short area can be determined as interference.

Step 4: Extract the edge from the target connected domain and calculate the interval between the edges of the wear surface of each row of contact wire as the contact wire wear surface width.

The process of measuring the wear plane width of contact wire is shown in Fig.8.

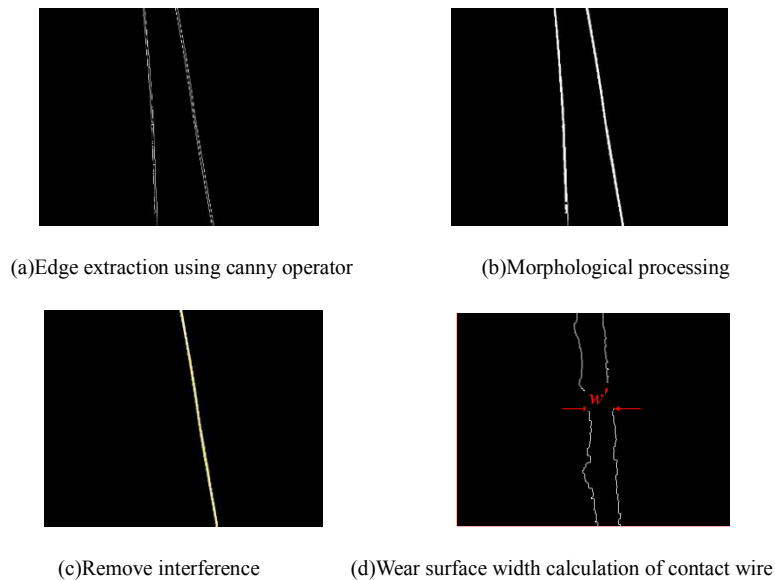


Fig.8. Calculation process of wear surface width of contact wire

After getting the value of w' and substituting it into the equation (6), the physical size of wear surface width of contact wire can be obtained.

Observe the cross section of contact wire as shown in Fig.9, and it is not difficult to see that the lower part of the wire is completely arc-shaped. As is known that the diameter of the lower part of the contact wire is 13.2 mm., the wear of contact wire is as follows:

$$d = r - \sqrt{r^2 - \left(\frac{w}{2}\right)^2} \tag{7}$$

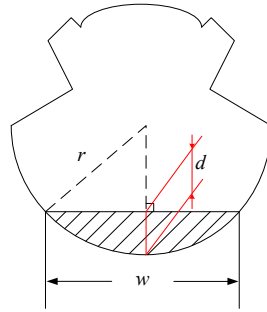


Fig.9. Cross section of contact wire

4. Data processing

4.1. Test of Zhengzhou-Kaifeng section

The commissioning test of the device is mainly carried out in the Zhengzhou-Kaifeng section of Longhai Line, and the measuring data of the entire line are sampled for analysis.

The group statistics on the wear data are performed, and according to the statistical result of Table 1 and the result distribution of Fig.10, it can be seen that 82.88% of contact wire wear in Zhengzhou-Kaifeng section of Longhai Line is distributed in the interval [0mm, 1.5mm]. The highest wear distribution of the whole line is around 1mm. Meanwhile, the percentage of the contact wire wear value exceeding the safety warning value 3.6mm only accounts for 0.22%.

Table 1 Statistics of contact wire wear d in Zhengzhou-Kaifeng section

Wear section height of contact wire (mm)	Data volume of monitoring line	Percentage of data (%)
$0 \leq d < 0.50$	12	0.01
$0.50 \leq d < 1.00$	23862	15.95
$1.00 \leq d < 1.25$	55462	37.07
$1.25 \leq d < 1.50$	29220	19.53
$1.50 \leq d < 1.75$	15445	10.32
$1.75 \leq d < 2.00$	11345	7.58
$2.00 \leq d < 2.25$	5388	3.60
$2.25 \leq d < 2.50$	4908	3.28
$2.50 \leq d < 3.00$	1820	1.22
$3.00 \leq d < 3.60$	1256	0.84
$3.60 \leq d < 4.50$	558	0.37
$4.50 \leq d < 6.45$	180	0.12
$d \geq 6.45$	144	0.10

In Fig.10, it presents the statistical curve of the wear data of contact wire in the Zhengzhou-Kaifeng section of Longhai Line, and it is easier to see from this curve that the wire wear of the entire Longhai Line is mainly distributed in a lower interval, and there are fewer phenomena of serious wear.

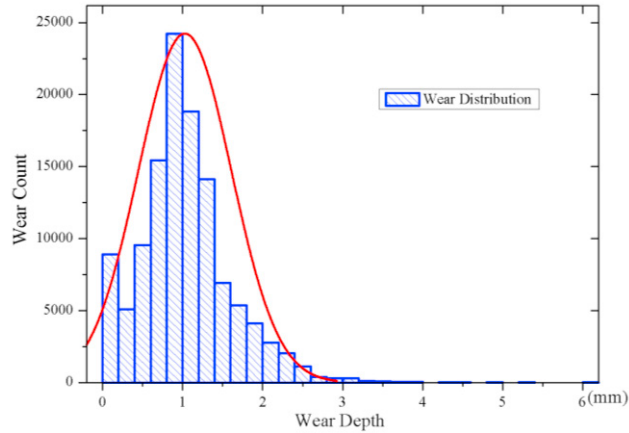


Fig.10. Statistics on the wear distribution of contact wire in Zhengzhou-Kaifeng section

4.2 Test of East Lechang -Shaoguan section

In the East Lechang -Shaoguan section of Longhai Line, the measuring data of whole line are sampled for analysis, and the analysis process is the same as the last test.

The results of Table 2 and Fig.11 are obtained by making the statistics on the distribution of wear data.

Table 2 Statistics of contact wire wear *d* in East Lechang -Shaoguan section

Wear section height of contact wire (mm)	Data volume of monitoring line	Percentage of data (%)
$0 \leq d < 0.50$	19	0
$0.50 \leq d < 1.00$	24752	14.06
$1.00 \leq d < 1.25$	57519	32.68
$1.25 \leq d < 1.50$	33567	19.07
$1.50 \leq d < 1.75$	22511	12.79
$1.75 \leq d < 2.00$	18913	10.75
$2.00 \leq d < 2.25$	8679	4.93
$2.25 \leq d < 2.50$	6382	3.63
$2.50 \leq d < 3.00$	1827	1.04
$3.00 \leq d < 3.60$	1062	0.60
$3.60 \leq d < 4.50$	453	0.26
$4.50 \leq d < 6.45$	178	0.10
$d \geq 6.45$	149	0.08

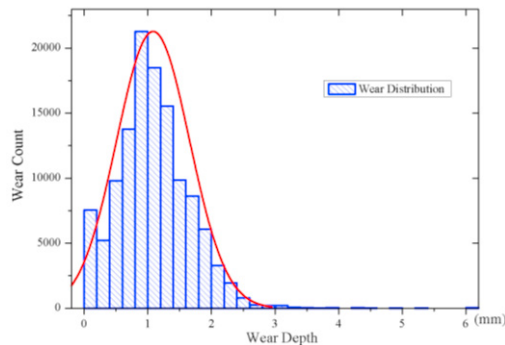


Fig.11. Statistics on the wear distribution of contact wire in East Lechang -Shaoguan section

From this curve, it is easier to see that the contact wire wear of East Lechang -Shaoguan section is also distributed in a lower interval, and the contact wire is in good condition. Through the analysis on the wear data of the whole line, especially the statistics of the distribution interval of the wire wear and combined with the image acquisition effect of the whole line, it can be seen that the contact wire wear of the whole line is in good condition and is monitored accurately by the system device, providing the certain reference for line repair and maintenance.

4.3 Uncertainty verification of measuring equipment

In order to verify the uncertainty of equipment, the wear analysis results of the measuring device are manually checked during the two tests, and 10 groups of data are collected and compared by the relevant on-site technical personnel.

Table 3 Wear data statistics in the first test (Zhengzhou-Kaifeng)

Measured data (mm)	Manual data (mm)	Uncertainty (mm)	Uncertainty (%)
0.938853	0.9	0.078853	4.31
1.105682	1.1	0.005682	0.51
1.552105	1.5	0.052105	3.47
1.637451	1.6	0.037451	2.34
1.242907	1.2	0.042907	3.57
1.315676	1.3	0.015676	1.20
1.105682	1.1	0.005682	0.51
1.242907	1.2	0.042907	3.57
1.105682	1.1	0.005682	0.51
1.041015	1.0	0.041015	4.10
0.938853	0.9	0.078853	4.31
1.105682	1.1	0.005682	0.51
1.552105	1.5	0.052105	3.47

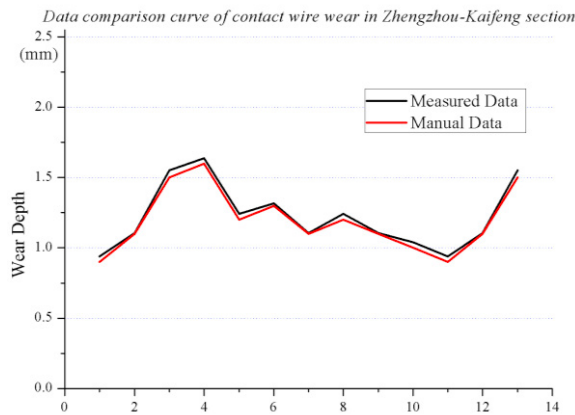


Fig.12. Local comparison of wear data of contact wire in Zhengzhou-Kaifeng section

Table 3 shows 10 sets of verification and comparison data collected by relevant on-site technicians after the catenary measuring vehicle departs from Zhengzhou Station 38 minutes and 34 seconds later in the test from Zhengzhou to Kaifeng. Table 4 shows 10 sets of verification and comparison data collected by relevant on-site technicians after the catenary measuring vehicle departs from East Lechang Station 17 minutes and 44 seconds later in the test from East Lechang to Shaoguan. From the data of two tables, it can be seen that the wear data of contact wire analyzed by the measured device are close to the data measured by manual on the site, and the uncertainty is within 5%.

Table 4 Wear data statistics in the second test (East Lechang-Shaoguan)

Measured data (mm)	Manual data (mm)	Uncertainty (mm)	Uncertainty (%)
2.385355	2.4	-0.01464	0.61
2.352345	2.3	0.052345	2.27
2.254558	2.2	0.054558	2.48
2.456246	2.5	-0.04375	1.75
2.508354	2.5	0.008354	0.33
2.189429	2.2	-0.01057	0.48
2.198493	2.2	-0.00151	0.06
2.346783	2.4	-0.05322	2.21
2.175433	2.1	0.075433	3.59
2.142357	2.1	0.042357	2.02
2.385355	2.4	-0.01464	0.61
2.352345	2.3	0.052345	2.27
2.254558	2.2	0.054558	2.48

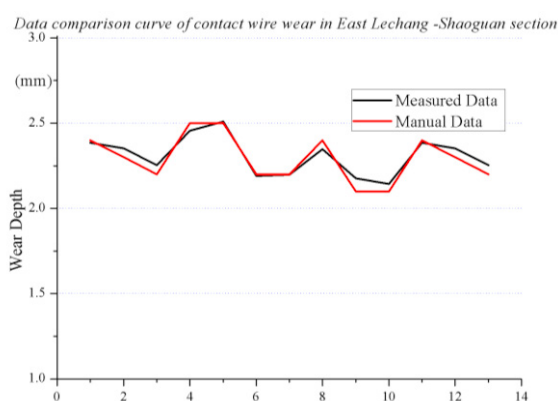


Fig.13. Local comparison of wear data of contact wire in East Lechang -Shaoguan section

From the data comparison curves of Fig.13 and Fig.13, it can be seen intuitively that the curves of real-time measuring data and manual data have better data repeatability, and the uncertainty of comparison data in the whole verification section is small. The device achieves the expected goal of the project, which can better complete the contact wire imaging in different wear conditions and calculate the wear depth of contact wire based on the algorithm.

5. Conclusion

Given the current condition of the increasing tension of contact wire and intensified local wear, through online test and corresponding artificial composite test, it is proved to be a feasible measurement method for the contact wire wear based on using the vision measuring equipment combined with binocular linear array camera and structured light.

Acknowledgement

The author would like to thank China Railway Guangzhou Administration Group Co., Ltd. for providing the test data, and he would also like to thank the anonymous reviewers for their valuable comments.

References

1. Qian Qingquan, Gao Shibin, He Zhengyou, et al. Key technologies of traction power supply for China high speed railway. *J Engineering Sciences* 2015;17(4):9-20.
2. Xu Chao, Yang Guangying. Analysis and improvement measures of wire breakage in catenary. *J Railway Quality Control* 2010; 38 (2): 19-20.
3. Chen Shaokuan, Wang Xiudan, Bai Yi, et al. Lowest costs-based optimum maintenance scheduling model for catenaries of railways. *J Journal of the China Railway Society* 2013; 35 (12): 37-42.
4. Sandhu R, Dambreville S, Tannenbaum A. Point set registration via particle filtering and stochastic dynamics. *J IEEE Transactions on Pattern Analysis & Machine Intelligence* 2010; 32(8):1459.
5. Liu Yan, Li Tengfei. Research of the improvement of Zhang's camera calibration method. *J Optical Technique* 2014; 40 (6): 565-570.
6. Liao Shuhong, Wu Jing, Zhang Haijun, et al. Pre-distortion technology for real-time correction of binocular digital image. *J Electronics optics&control* 2018 (5).
7. Cheng J T, Zhao C, Zhao W L, et al. Research and realization of a new algorithm for stereo matching based on binocular vision. *J Advanced Materials Research* 2013; 670:202-207.